International Journal of Nanomedicine

Dovepress
open access to scientific and medical research

Open Access Full Text Article

ORIGINAL RESEARCH

Electroactive $BaTiO_3$ nanoparticle-functionalized fibrous scaffolds enhance osteogenic differentiation of mesenchymal stem cells

This article was published in the following Dove Press journal:
International Journal of Nanomedicine
26 May 2017
Number of times this article has been viewed

Yiping Li,[1,2] Xiaohan Dai,[1] Yunyang Bai,[2] Yun Liu,[2] Yuehong Wang,[1] Ousheng Liu,[1] Fei Yan,[1] Zhangui Tang,[1] Xuehui Zhang,[3–5] Xuliang Deng[2,4,5]

[1]Department of Prosthodontics, Xiangya Stomatological Hospital & School of Stomatology, Central South University, Changsha, [2]Department of Geriatric Dentistry, [3]Department of Dental Materials & Dental Medical Devices Testing Center, Peking University School and Hospital of Stomatology, [4]National Engineering Laboratory for Digital and Material Technology of Stomatology, [5]Beijing Laboratory of Biomedical Materials, Peking University School and Hospital of Stomatology, Beijing, People's Republic of China

Correspondence: Zhangui Tang
Xiangya Stomatological Hospital & School of Stomatology, Central South University, 72 Xiangya Road, Changsha 410078, People's Republic of China
Tel +86 731 8480 5480
Fax +86 731 8480 5480
Email tangzhanguixiangya@163.com

Xuehui Zhang
Department of Dental Materials & Dental Medical Devices Testing Center, Peking University School and Hospital of Stomatology, Zhongguancun South Avenue No 22, Beijing 100081, People's Republic of China
Tel +86 10 8219 5748
Fax +86 10 6216 4691
Email zhangxuehui914@163.com

Abstract: It has been proven that the surface topographic cues of fiber arrangement can induce osteogenic differentiation of mesenchymal stem cells. However, this effect alone is weak and insufficient to meet the needs of regenerative medicine. In this work, electroactivity concept was introduced to enhance the osteoinductivity of fibrous scaffolds. The randomly oriented and aligned electroactive fibrous scaffolds of poly-(L-lactic acid) (PLLA) with incorporation of ferroelectric ceramic $BaTiO_3$ (BTO) nanoparticles (NPs) were fabricated by electrospinning. Physicochemical properties, including fiber morphology, microstructure, composition, thermal stability, surface roughness, and surface wettability, of these fibrous scaffolds were studied. The dielectric properties of the scaffolds were evaluated. The results showed that the randomly oriented BTO/PLLA composite fibrous scaffolds had the highest dielectric permittivity of 1.19, which is of the same order of magnitude as the natural bone. The combined effects of fiber orientation and electrical activity on the osteogenic responses of bone marrow mesenchymal stem cells (BM-MSCs) were specifically investigated. Randomly oriented composite fibrous scaffolds significantly promoted polygonal spreading and encouraged early osteogenic differentiation in BM-MSCs, whereas aligned composite fibrous scaffolds promoted cell elongation and discouraged osteogenic differentiation. These results evidenced that randomly fiber orientation and biomimetic electric activity have combining effects on osteogenic differentiation of BM-MSCs. Our findings indicate that coupling effects of multi-physical properties should be paid more attention to mimic the microenvironment for enhancing osteogenic differentiation of BM-MSCs.

Keywords: topographic substrate, biomimetic electroactivity, ferroelectric ceramic, polarization, osteogenic responses

Introduction

Numerous studies have shown that topographic cues of fiber arrangement can regulate stem cell behaviors such as cell attachment, spreading, growth, and differentiation via contact guidance.[1–4] Randomly oriented fibrous scaffolds could typically encourage osteogenic differentiation, and aligned fibrous scaffolds could promote myogenic or neurogenic differentiation in stem cells.[5–7] Our previous researches showed that electrospun poly-(L-lactic acid) (PLLA) fiber orientation played an important role in regulating osteoblast response and confirmed that bone marrow mesenchymal stem cells (BM-MSCs) cultured on randomly oriented PLLA nanofibers showed enhanced osteogenic-specific fate compared with those cultured on aligned nanofibers.[8,9] Yin et al demonstrated that osteogenesis in vivo was driven by randomly oriented electrospun PLLA fiber scaffolds.[10]

submit your manuscript | www.dovepress.com
Dovepress
http://dx.doi.org/10.2147/IJN.S135605

However, the extent of osteogenic differentiation on the randomly oriented fibrous scaffolds alone was lower than that driven by the chemical induction medium. Therefore, how to magnify the effect of surface topographic cues of randomly oriented fibers on osteogenic differentiation of MSCs would be of substantial interest.

Electrical effects such as piezoelectricity, pyroelectricity, and dielectricity play an important role in bone growth, remodeling, and fracture healing.[11–14] Recently, ferroelectric ceramics, including lithium niobate (LN)[15–17] and barium titanate ($BaTiO_3$ [BTO]),[18–20] have been widely used as bone repair materials with excellent biocompatibility and osseointegration, because of relatively high spontaneous polarization and an inherent ability to sustain a charged surface. In our recent study, BTO nanoparticles (NPs) have been incorporated into the polymer matrix to achieve positive bone-defect repair efficiency due to its inherent and sustainable electrical activity mimicking physiological electrical properties.[21] So, the incorporation of an electroactive component into the PLLA fibrous scaffolds may be an alternative to magnify the topological regulation effect on mesenchymal stem cell osteogenic responses.

The purpose of this study was to explore the combining effects of biomimetic electroactivity and surface topological structure of fibrous scaffolds on mesenchymal stem cell osteogenic responses. In this work, we chose PLLA as the material matrix and BTO NPs as electroactive fillers to fabricate randomly oriented and aligned composite fibrous scaffolds by electrospinning. The physicochemical properties, including fiber morphology, microstructure, chemical composition, thermal stability, surface roughness, and surface wettability of the fibrous scaffolds, were investigated. Dielectric behavior was studied at room temperature to determine the electrical properties of the fibrous scaffolds. Additionally, BM-MSCs were used to evaluate and compare the biological performance (cell attachment, cell proliferation, and early osteogenic differentiation) of the fibrous scaffolds.

Materials and methods

Preparation of electrospun BTO/PLLA composite fibrous scaffolds

Before the BTO NPs were incorporated into the PLLA matrix, surface modification of BTO was performed. Briefly, a defined amount of BTO NPs (average particle size of 100 nm; Alfa Aesar, Ward Hill, MA, USA) was dispersed in deionized water containing 2% w/v sodium citrate. The surface-modified BTO NPs and PLLA (Mw =10×10^4; Shan Dong Institute of Biomedical Instruments, Shandong, People's Republic of China) were then proportionally dispersed in the trifluoroethanol (TFE) solution by ultrasonication for 2 h, followed by stirring for 12 h, to form a stable suspension. The BTO contents were set as 1, 3, 5, 7, and 10 wt% of the PLLA. Thereafter, as described in Figure 1, electrospinning was then performed using two different collectors – the plate and rolling collectors – with preset parameters, including applied voltage, solution feeding rate, and collecting distance. Finally, randomly oriented BTO/PLLA microfibers (BTO/PLLA RM) and aligned BTO/PLLA composite microfibers (BTO/PLLA

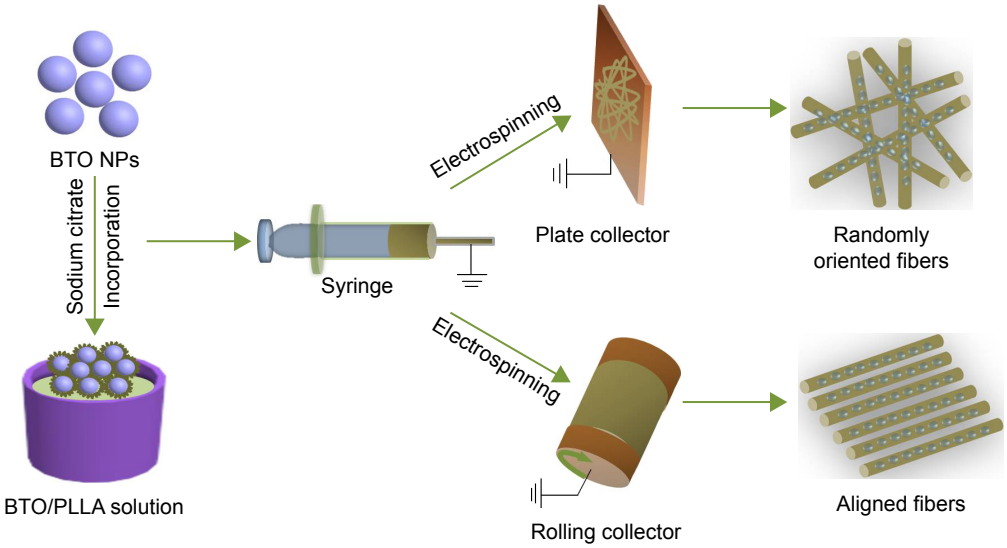

Figure 1 Schematic diagram of the fabrication process of electrospun BTO/PLLA composite fibrous scaffolds.
Notes: BTO NPs were modified by sodium citrate solution and then proportionally dispersed into the PLLA solution to form BTO/PLLA solution. Thereafter, electrospinning was performed using two different collectors – plate and rolling collectors – under preset parameters. Randomly oriented and aligned BTO/PLLA composite fibrous scaffolds, respectively, were thereby fabricated.
Abbreviations: BTO, $BaTiO_3$; PLLA, poly-(L-lactic acid); NP, nanoparticle.

AM) were obtained. All electrospun fibrous scaffolds, including randomly oriented neat PLLA microfibers (PLLA RM), aligned neat PLLA microfibers (PLLA AM), BTO/PLLA RM and BTO/PLLA AM, were dried for 3–4 days in a vacuum oven to remove any residual solvents.

Characterization of electrospun fibrous scaffolds

The surface morphology and microstructural features of the composite fibers were observed using a scanning electron microscope (SEM; Hitachi, S-4700, Hitachi Ltd., Tokyo, Japan). The distribution of BTO NPs in the PLLA fibrous matrix was investigated by transmission electron microscopy (TEM; Hitachi H-800). Fiber diameter was measured from the SEM photographs by using image analysis software (ImageJ; National Institutes of Health, Bethesda, VA, USA). Chemical compositions of the composite fibers were evaluated by energy-dispersive X-ray spectroscopy (EDS; EMAX EX-300 system), X-ray diffraction (XRD; Rigaku D/max 2500 VB2+/PC), and thermogravimetric analysis (TGA; STA 449C). The surface roughness of the scaffolds was examined by an Omniscan MicroXAM white light interferometer (ADE Phase Shift, Tucson, AZ, USA), and the resulting data were analyzed using the MapVUE AE software (Meta MAP, Lexington, KY, USA). The surface wettability of the samples was assessed by water contact angle measurements performed on a video contact angle instrument (JC2000C1; Shanghai Glory Numeral Technique & Device Co., Ltd., Shanghai, People's Republic of China). The dielectric property of samples was measured on a HP 4294A precision impedance analyzer (Agilent Technologies, Santa Clara, CA, USA) at room temperature.

Cell culture

Rat BM-MSCs (Cyagen Bioscience Inc., Guangzhou, People's Republic of China) were cultured in Dulbecco's Modified Eagle's Medium (DMEM) supplemented with 10% fetal bovine serum (FBS) and 100 IU/mL penicillin–streptomycin. The medium was changed every 2–3 days. At 80%–90% confluence, BM-MSCs were detached using 0.25% trypsin/ethylenediaminetetraacetic acid (EDTA; Gibco, Grand Island, NY, USA). Cells from passages 3 to 5 were used for the following experiments.

Attachment and proliferation of BM-MSCs on fibrous scaffolds

BM-MSCs were seeded onto experimental scaffolds in 12-well plates (5×10^4 cells/well) and incubated at 37°C in a humidified atmosphere with 5% CO_2. After 1 or 5 days of culture, the samples were fixed in 2.5% glutaraldehyde and serially dehydrated in an increasing ethanol gradient, air-dried in a hood, and sputtered with gold prior to SEM imaging. Cell spreading area and cell elongation were measured using the ImageJ software, by using a random sampling method. For cytoskeleton observation, the attached cells after 5 days of culture were fixed with 4% paraformaldehyde, incubated with Alexa Fluor 546 phalloidin (50 μg/mL) for 1 h and stained with 4′, 6-diamidino-2-phenylindole (DAPI) for 10 min according to the manufacturer's directions. The images were captured by a confocal laser scanning microscopy (CLSM; CLSM 780; Carl Zeiss Jena GmbH, Jena, Germany). Cell proliferation was assayed using a Cell Counting Kit-8 (CCK-8 kit, Dojindo Laboratory, Tokyo, Japan) at 1, 3, 5, and 7 days of culture, with absorbance being read at a wavelength of 450 nm, by using an enzyme linked immunosorbent assay reader (Bio-Rad, Hercules, CA, USA).

Osteogenic differentiation of BM-MSCs on fibrous scaffolds

The specific osteogenic marker runt-related transcription factor 2 (RUNX-2) was detected by immunofluorescence staining as described in our previous study.[22] BM-MSCs were cultured on the randomly oriented and aligned fibrous scaffolds in 12-well plates (5×10^4 cells/well) for 5 days. The samples were then fixed in 4.0% paraformaldehyde for 15 min at room temperature and washed three times with phosphate-buffered saline (PBS). The cells were then permeabilized with 0.1% Triton X-100 in PBS for 5 min, washed three times with PBS, and blocked with 5% bovine serum albumin (BSA) for 1 h. Subsequently, the cells were incubated with the RUNX-2 primary antibody (diluted 1:100; Abcam, Cambridge, MA, USA) overnight at 4°C. After thorough rinsing to remove excess primary antibody, cells were further incubated with a 1:500 dilution of the secondary antibody (fluorescein isothiocyanate-conjugated AffiniPure Goat Anti-mouse IgG; Abcam) for 2 h at ambient temperature. Finally, cells were treated with Alexa Fluor 546 phalloidin (50 μg/mL) for 1 h at room temperature, and cell nuclei were stained with DAPI for 10 min. Images of the stained cells were then acquired using CLSM. The mean fluorescence intensities of positive RUNX-2 expression were analyzed using Image-Pro Plus Software (Media Cybernetics, Sliver Spring, MD, USA). The measurement was performed for a minimum of 100 cells on each group. For alkaline phosphatase (ALP) activity assay, an Alkaline Phosphatase Assay Kit (Abcam) was utilized. BM-MSCs were cultured on the randomly oriented and aligned fibrous scaffolds in 12-well plates (5×10^4 cells/well) for 5 days. Culture supernatants were incubated with alkaline buffer and

p-nitrophenyl phosphate for 60 min according to the manufacturer's instructions, and then the reaction was terminated with the stop solution. The absorbance was measured at a wavelength of 405 nm, and the values of ALP activity were read off a standard curve based on standard samples provided with the kit.

Statistical analysis

All quantitative data were expressed as mean ± standard deviation (SD). Statistical analyses were performed using the SPSS 13.0 software (SPSS Inc., Chicago, IL, USA). Statistical differences were determined using Student's *t*-test for independent samples. Differences between groups with $P<0.05$ were considered as statistically significant, and $P<0.01$ was considered as highly significant.

Results and discussion

Surface morphologies and compositions of electrospun fibrous scaffolds

The optimal BTO NP content in the PLLA fibrous matrix was first determined. As shown in Figure 2A, neat PLLA fibers were continuous, smooth, and homogeneous. When 1 wt% BTO NPs were incorporated in PLLA fibers, little and uneven BTO NPs dispersed in the PLLA fibers (Figure 2B) were observed. This may directly affect the electrical property of fibrous scaffolds due to the lack in homogeneity of BTO distribution. In the composite fibers with 3 and 5 wt% BTO NPs, apparent BTO NP aggregates and inhomogeneous nanofibers were observed (Figure 2C and D). When the content of BTO NPs was increased to 7 wt%, homogeneous composite fibers were achieved (Figure 2E). When the concentration of BTO NP fillers was increased to 10 wt%, a number of beads were seen and the fibers were discontinuous (Figure 2F). Moreover, incorporation of BTO NPs reduced fiber diameter, but this reduction did not show a dose dependence. This reduction in the composite fiber diameter may be due to the decrease in solution viscosity after the incorporation of BTO NPs and the unevenness of the forces between the agglomerated BTO NPs and the polymer derived from high electric fields applied in the electrospinning process. Furthermore, it can be seen from Figure 3 that BTO NPs were not only dispersed in the fiber matrix uniformly in the composite fibers with 7 wt% BTO NPs (Figure 3A) but also were embedded in the fibers, as proved by the TEM image (Figure 3B). The presence of BTO NPs in composite was further confirmed by EDS spectra (the inset of Figure 3A). Thus, composite fibers with 7 wt% BTO NPs were considered optimal and used in following experiments.

Based on our abovementioned findings, randomly orientated and aligned BTO/PLLA composite fibrous scaffolds with the same content of BTO NPs of 7 wt% were fabricated to compare the effects of fiber orientation on scaffold electrical properties and biological performance. As shown in Figure 4A, randomly oriented and aligned neat PLLA fibers exhibited uniformly smooth surfaces. The randomly oriented BTO/PLLA fibers showed isotropic fiber alignments, whereas aligned composite fibers exhibited anisotropic

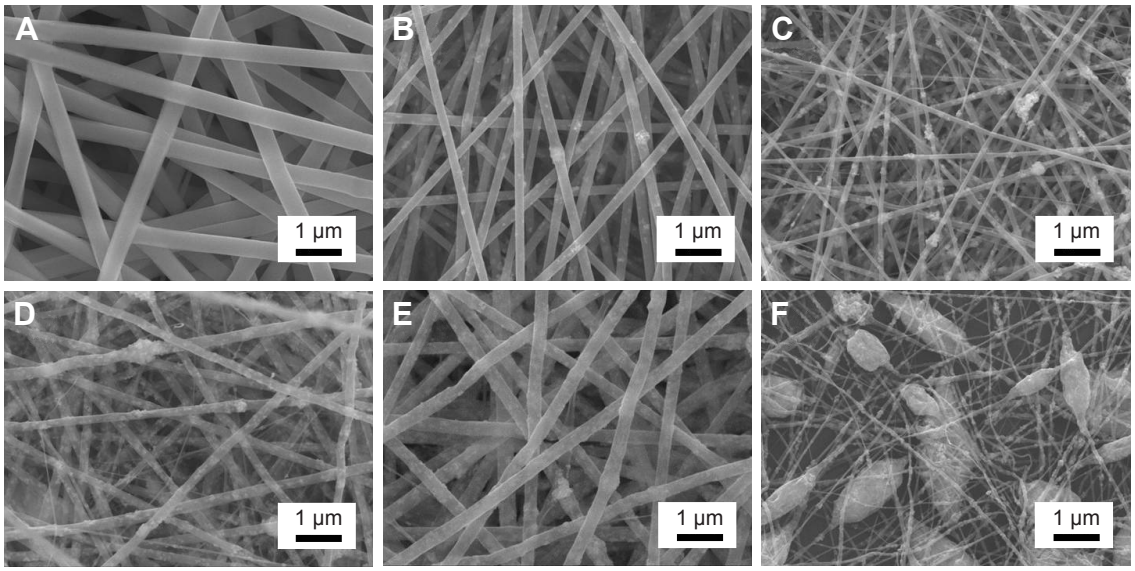

Figure 2 SEM images of electrospun randomly oriented BTO/PLLA composite fibrous scaffolds with different BTO NP content.
Notes: (**A**) Neat PLLA fibers, (**B**) 1 wt% BTO NPs, (**C**) 3 wt% BTO NPs, (**D**) 5 wt% BTO NPs, (**E**) 7 wt% BTO NPs, and (**F**) 10 wt% BTO NPs.
Abbreviations: SEM, scanning electron microscope; BTO, $BaTiO_3$; PLLA, poly-(L-lactic acid); NP, nanoparticle.

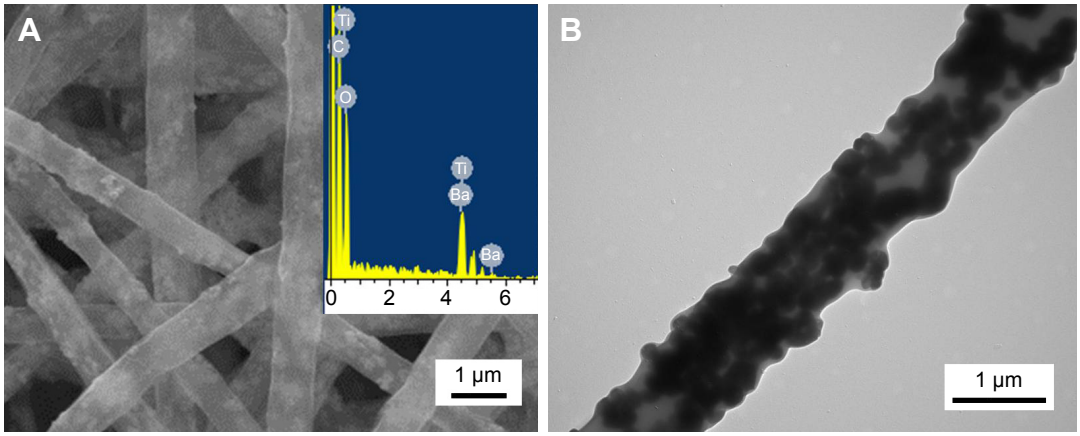

Figure 3 Morphology and microstructure of electrospun randomly oriented BTO/PLLA composite fibers with 7 wt% BTO NPs.
Notes: (**A**) SEM image at a high magnification and EDS spectra. (**B**) TEM image of BTO NPs distributed in the PLLA fibers.
Abbreviations: BTO, $BaTiO_3$; PLLA, poly-(L-lactic acid); NP, nanoparticle; SEM, scanning electron microscope; EDS, energy-dispersive X-ray spectroscopy; TEM, transmission electron microscopy.

alignments. The results of fiber-diameter distribution analysis are shown in Figure 4B. Generally, the average diameters of randomly oriented fibers were higher than those of aligned fibers, which could be due to the secondary stretching effects during collection in the high-speed rational receiving drum. The diameters of the randomly oriented neat PLLA fibers were ~1,177±119 nm; however, the diameters of the aligned neat PLLA fibers decreased to 574±88 nm. The incorporation of BTO NPs decreased the fiber diameter; the diameters of the randomly oriented BTO/PLLA composite fibers were 722±172 nm and those of the aligned BTO/PLLA composite fibers were further lowered to 311±65 nm. This was mainly due to the difference in the viscosities of the initial suspensions. As the dispersion of BTO NPs in composite solutions could destruct the molecular polymer links, the viscosity of solution could be reduced by incorporation of BTO NPs, leading to decreased electrospun fiber diameter.

Crystal structure and thermal stability of composite fibrous scaffolds

Figure 5A shows the XRD patterns of the various fibrous scaffolds and BTO NPs. Pure tetragonal phase was detected in BTO NPs and BTO/PLLA composite fibers. Moreover, the structure of PLLA was not affected by the incorporation of BTO NPs and the electrospinning process. The thermal stability of the fibrous scaffolds was further evaluated by TGA. As shown in

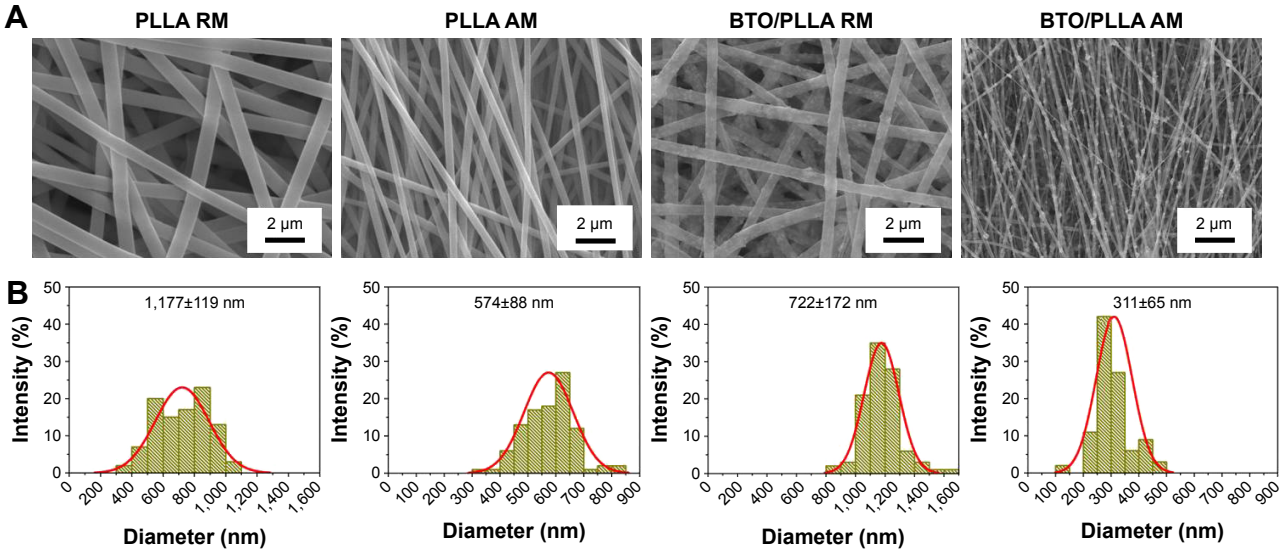

Figure 4 SEM images of electrospun randomly oriented or aligned fibrous scaffolds and their diameter distribution histograms.
Notes: (**A**) SEM images. (**B**) Diameter distribution histograms.
Abbreviations: SEM, scanning electron microscope; PLLA RM, randomly oriented neat PLLA microfibers; PLLA AM, aligned neat PLLA microfibers; BTO/PLLA RM, randomly oriented BTO/PLLA microfibers; BTO/PLLA AM, aligned BTO/PLLA composite microfibers; PLLA, poly-(L-lactic acid); BTO, $BaTiO_3$.

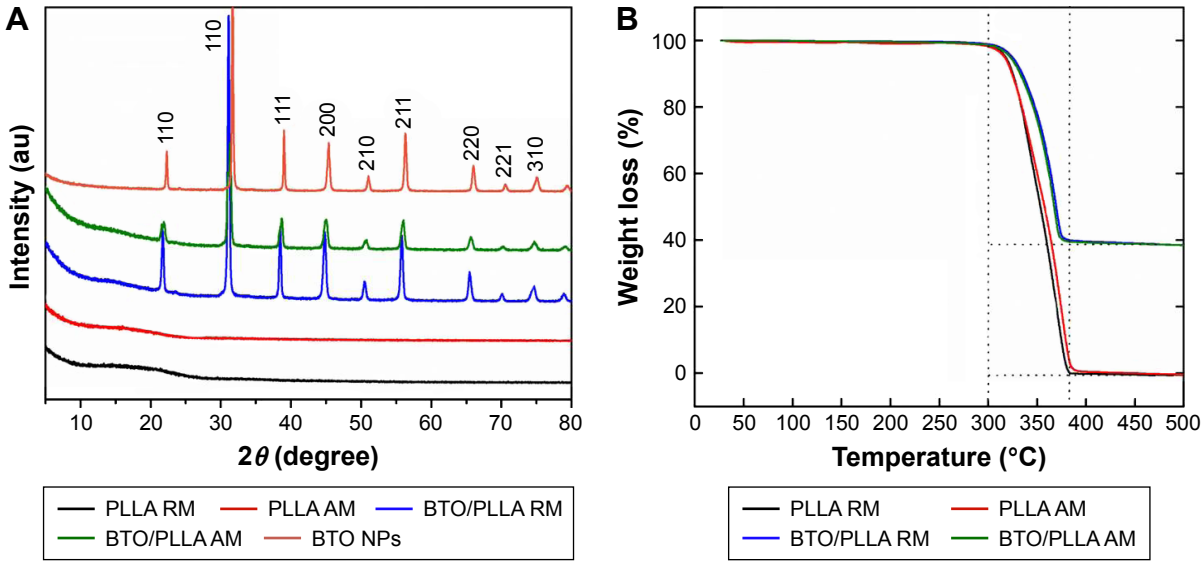

Figure 5 XRD patterns (**A**) and TGA spectra (**B**) of the different electrospun fibrous scaffolds.
Abbreviations: XRD, X-ray diffraction; TGA, thermogravimetric analysis; PLLA RM, randomly oriented neat PLLA microfibers; BTO/PLLA RM, randomly oriented BTO/PLLA microfibers; PLLA AM, aligned neat PLLA microfibers; BTO/PLLA AM, aligned BTO/PLLA composite microfibers; NP, nanoparticle; PLLA, poly-(L-lactic acid); BTO, $BaTiO_3$.

Figure 5B, a significant weight loss was observed at ~300°C, associated with degradation and combustion of the PLLA component. At ~380°C, the weight loss of both randomly oriented and aligned PLLA fibrous scaffolds changed to zero, while the weight loss of composite fibrous scaffolds remained ~40% and no longer reduced until 500°C. The results suggested that both randomly oriented and aligned BTO/PLLA fibrous scaffolds have excellent thermal stability and that fiber orientation did not affect the thermal stability of composite scaffolds.

Surface roughness and surface wettability of composite fibrous scaffolds

The surface roughness and surface wettability of fibrous scaffolds were then investigated. A white light interferometer was used to examine the surface roughness by scanning the surface morphology of fiber meshes. As shown in Figure 6A, BTO/PLLA composite fibrous scaffolds had a significantly higher surface roughness than did neat PLLA fibrous scaffolds. This may be ascribed to the rough fiber surface created by incorporated BTO NPs as shown in Figure 3. Furthermore, the randomly oriented composite fibrous scaffolds had a higher surface roughness than that of the aligned scaffolds. This may be explained by the concept that BTO NPs in the randomly oriented fibers were less constrained by the polymer fibers than those in the aligned fibers, resulting in more protrusions on the fiber surface. This result also suggested that the random fiber configuration of composite fibrous scaffolds helps to enhance their surface roughness.

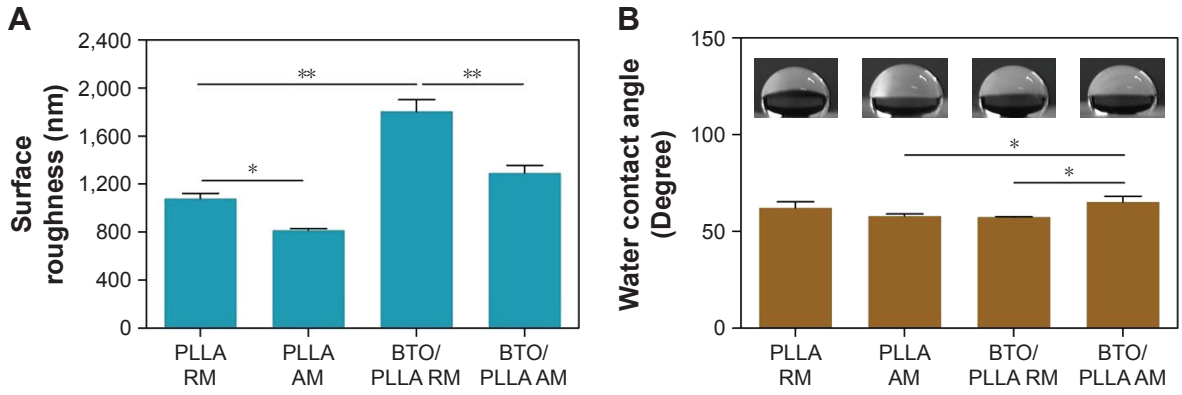

Figure 6 Surface roughness (**A**) and water contact angle (**B**) of different electrospun fibrous scaffolds.
Notes: The insets of Figure 6B are the photograph of water contact angle. *$P<0.05$; **$P<0.01$.
Abbreviations: PLLA RM, randomly oriented neat PLLA microfibers; PLLA AM, aligned neat PLLA microfibers; BTO/PLLA RM, randomly oriented BTO/PLLA microfibers; BTO/PLLA AM, aligned BTO/PLLA composite microfibers; PLLA, poly-(L-lactic acid); BTO, $BaTiO_3$.

Figure 6B shows the surface wettability of fibrous scaffolds. The water contact angles of all the fiber scaffold samples were <80° and had no correlation with BTO incorporation and fiber orientation. There was no significant difference between the neat randomly oriented and aligned PLLA samples. After incorporation of BTO NPs, however, randomly oriented composite fibrous scaffolds had lower water contact angles that those of aligned composite samples and neat PLLA samples, which indicates that the incorporation of BTO NPs and isotropy of fibers synergistically improved the surface hydrophilicity of composite fibrous scaffolds. The improved surface hydrophilicity was also ascribed to the enhancement of surface roughness derived from micro- or nanoscale fibrous structure and protrusions of BTO NPs. It has been reported that the wettability of the surface depends on the surface energy and the roughness of the surface.[23] It has also been confirmed that the microscale and nanoscale roughness could increase the hydrophobicity of the surface.[24] Numerous studies have demonstrated that enhanced surface roughness and surface hydrophilicity could improve the biocompatibility of scaffold materials.[25–27] Therefore, these results imply that BTO/PLLA composite fibrous scaffolds might exhibit favorable biological performance.

Electrical properties of composite fibrous scaffolds

Electrical signals are involved in all functions of living cells and organisms.[28,29] Electroactive micro-/nanofibrous scaffolds are therefore of great interest in the field of scaffold design because of their three-dimensional microenvironment structure as well as their electrical stimulation effects.[30–32] In our work, therefore, we attempted to integrate the inherent electroactive component into PLLA fibrous matrix to form a highly biomimetic composite scaffold material. The frequency-dependent dielectric permittivity results of different fibrous scaffolds are shown in Figure 7. Generally, the dielectric permittivity of randomly oriented fibrous scaffolds was significantly higher than that of aligned fibrous scaffolds. Furthermore, the randomly oriented BTO/PLLA composite fibrous scaffolds had a higher dielectric permittivity than the randomly oriented neat PLLA fibrous scaffolds did, which was in agreement with a previous report.[33] BTO NPs

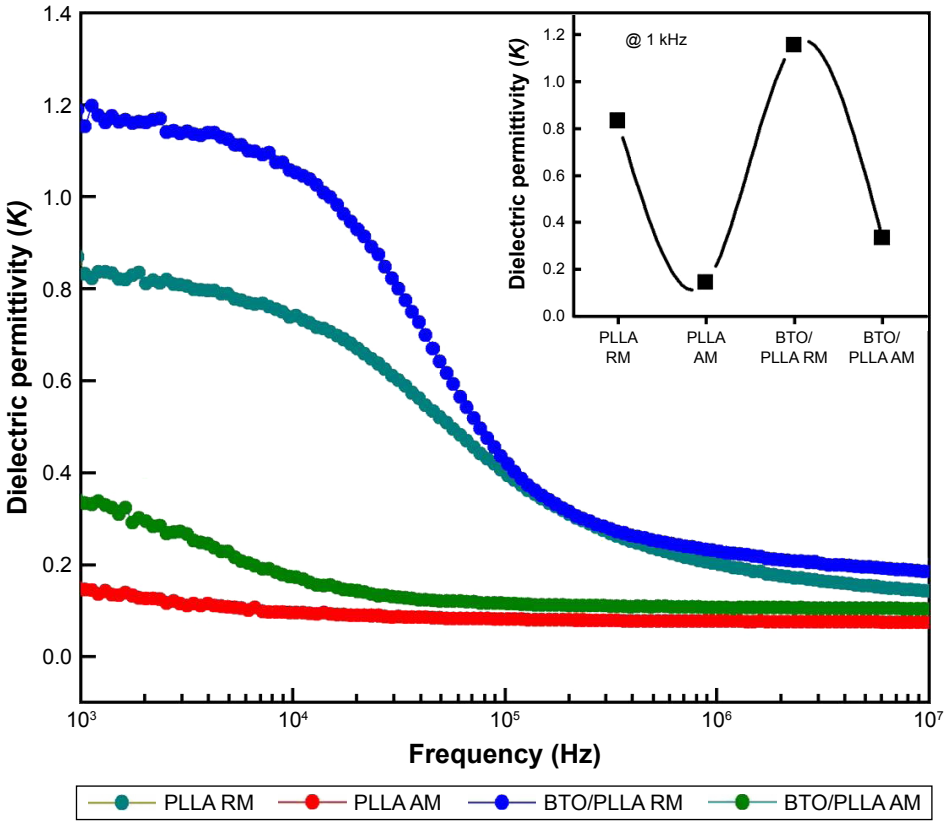

Figure 7 Effects of BTO NPs and fiber orientation on the dielectric permittivity of electrospun composite BTO/PLLA fibrous scaffolds.
Note: Superimposed in the inset is the dielectric permittivity measured at 1 kHz at room temperature.
Abbreviations: BTO, $BaTiO_3$; NP, nanoparticle; PLLA, poly-(L-lactic acid); PLLA RM, randomly oriented neat PLLA microfibers; PLLA AM, aligned neat PLLA microfibers; BTO/PLLA RM, randomly oriented BTO/PLLA microfibers; BTO/PLLA AM, aligned BTO/PLLA composite microfibers.

have usually been used as ceramic fillers to enhance the dielectric performance of polymer composites due to their high dielectric constants.[34–37] BTO is also a particularly attractive ferroelectric ceramic material for application in the biomedical field owing to its biocompatibility and capability of spontaneous polarization.[38–40] In our work, the measured dielectric permittivity of randomly oriented composite fibrous scaffolds was ~1.19±0.02, which was close to the measured value (1.1±0.03) and the theoretical calculated value (1.14) reported by Morvan et al.[33] The dielectric constant value was also within the same order of magnitude as the dielectric constant value of dry human bone.[41,42]

The improved dielectric property could be mainly due to poling of the ferroelectric BTO NPs during the electrospinning process. According to the description of Morvan et al,[33] BTO NPs can easily rotate during the initial stages of the spinning process before the solvent completely evaporates, after which they get progressively locked by the hardening PLLA matrix in the orientation of the polarization derived from high electric fields applied in the electrospinning process. In principle, the highly disordered interfacial regions between the nanoscale BTO NPs and PLLA matrix are effective traps for space charges, such as ions or free electrons.[35,43,44] Upon the application of a poling electric field, these space charges migrate along the directions of the electric field and form large dipoles, giving rise to enhanced electrical polarization.[36]

Therefore, the dielectric constant of BTO/PLLA composite fibrous scaffolds markedly increased after incorporation of BTO NPs. However, the dielectric property of aligned composite fibrous scaffolds was not significantly improved, which could be attributed to the effect of fiber orientation on electrical polarization of BTO NPs in composite fibers during the electrospinning process. These results imply that randomly oriented BTO/PLLA composite fibrous scaffolds might have the ability to provide a biomimetic electrical microenvironment for cell function and differentiation.

Attachment, spreading, and proliferation of BM-MSCs on charged fibrous scaffolds

The biological performance of electrospun composite fibrous scaffolds was further investigated. The morphology of BM-MSCs after 24 h cultivation on different fibrous scaffolds is shown in Figure 8A. The cells cultured on the randomly oriented fibrous scaffolds showed polygonal forms with many filopodia-like extensions and filament-like structures, whereas elongated and polarized cell morphology with orientations along the fiber directions were observed on the aligned fibrous scaffolds. This is consistent with our previous studies.[8,9] As shown in Figure 8B, the wide spreading of cellular actin filaments was most obvious on the randomly oriented BTO/PLLA composite fibrous scaffolds, while the directionally orientated cellular actin filaments were seen on the aligned neat PLLA and aligned BTO/PLLA composite fibrous scaffolds. Furthermore, cells on the randomly oriented BTO/PLLA composite fibrous scaffolds showed the most increased cell spreading area in comparison with those on the randomly oriented neat PLLA fibrous scaffolds and aligned neat PLLA and aligned BTO/PLLA composite fibrous scaffolds (Figure 8C), while the aligned BTO/PLLA composite fibrous scaffolds showed a slightly enhanced cell elongation (Figure 8D). These results indicate that incorporation of BTO NPs into randomly oriented composite fibrous scaffolds further promoted the spreading of BM-MSCs.

Large cell spreading area and polygonal cell shape with much filopodia are closely related with the osteogenic activity of MSCs.[8,9,45–48] The topographical structure and electric activity of randomly oriented fibers have combining effects on the behavior of BM-MSCs. The involved mechanism may be explained as two aspects: the first is the contact guidance effect of the topological structure of the fibrous scaffold on cellular behaviors and the second is the electrotaxis effect inspired by the dielectricity of BTO NPs. The classical theory of contact guidance has been used to explain the morphological phenotypes of MSCs on different topographic nanofibers in our previous studies.[8,9] The electrotaxis effect inspired by the electroactivity of BTO NPs has also been confirmed by our recent report – the migration ability of BM-MSCs in polarized nanocomposite membranes with BTO NPs was significantly enhanced compared with that of neat membranes without BTO NPs.[21]

As shown in Figure 8E, cell proliferation was assessed using a CCK-8 assay after 1, 3, 5, and 7 days of culture. The cell number increased steadily throughout the culture period. Furthermore, composite fibrous scaffolds with either random or aligned orientation promoted cell proliferation in comparison to neat fibrous scaffolds. This effect was largely related to increased surface roughness and surface hydrophilicity due to BTO NP incorporation, as well as improved electrical property. However after 5 days of culture, the cell proliferation rate became slightly slow on randomly oriented BTO/PLLA composite scaffolds and showed no significant difference from that of neat PLLA nanofibrous scaffolds by day 7. This was likely because more cells proliferated on the randomly oriented BTO/PLLA composite fibrous scaffolds, resulting in contact inhibition, as confirmed by SEM images (Figure 8A)

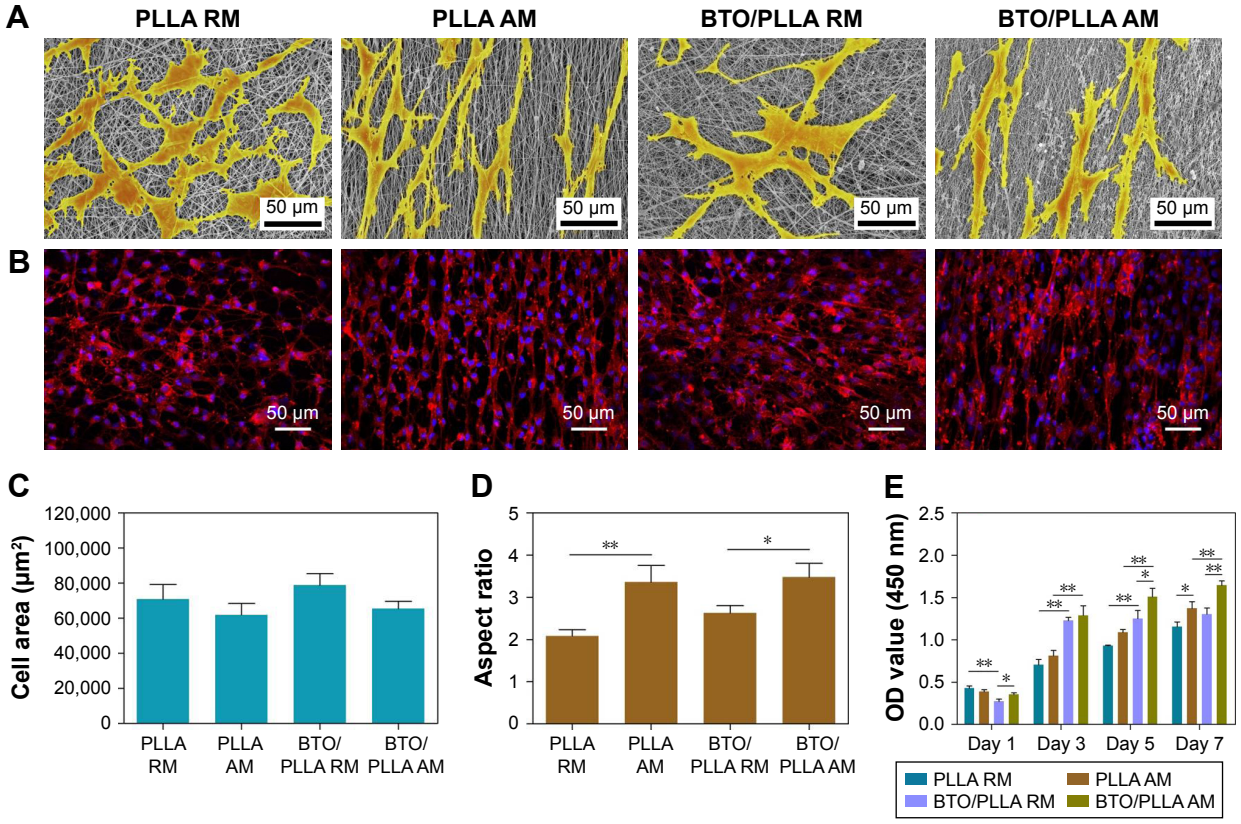

Figure 8 Attachment, spreading, and proliferation of BM-MSCs on different electrospun fibrous scaffolds.

Notes: (**A**) Representative SEM images of cell spreading of BM-MSCs cultured for 24 h. (**B**) Representative cytoskeleton images of BM-MSCs after 5 days of culture. (**C**) Quantitative analysis of cell spreading area after 1 day of culture. (**D**) Quantitative analysis of cell elongation after 24 h of culture. (**E**) Cell proliferation histograms after culture for 1, 3, 5, and 7 days (*$P<0.05$ and **$P<0.01$).

Abbreviations: ALP, alkaline phosphatase; BM-MSC, bone marrow mesenchymal stem cell; SEM, scanning electron microscope; PLLA RM, randomly oriented neat PLLA microfibers; PLLA AM, aligned neat PLLA microfibers; BTO/PLLA RM, randomly oriented BTO/PLLA microfibers; BTO/PLLA AM, aligned BTO/PLLA composite microfibers; PLLA, poly-(L-lactic acid); BTO, $BaTiO_3$; OD, optical density.

and CLSM images (Figure 8B). This slight proliferation suppressive effect is also possibly related to the differentiation tendency of BM-MSCs, because there is a reciprocal relationship between cell proliferation and differentiation.[49]

Osteogenic differentiation of BM-MSCs on charged fibrous scaffolds

To further confirm the effect of fiber orientation and BTO NP incorporation on early osteogenic differentiation ability of BM-MSCs, the production of RUNX-2 (a key transcription factor for bone formation) was studied by immunofluorescence staining as shown in Figure 9. We observed the highest positive expression of RUNX-2 on randomly oriented BTO/PLLA composite fibrous scaffolds than on others kinds of fibrous scaffolds after 5 days of culture (Figure 9A). Qualitatively, randomly oriented neat PLLA fibrous scaffolds generated a slightly higher fluorescence intensity than the aligned neat PLLA fibrous scaffolds. As expected, randomly oriented BTO/PLLA composite fibrous scaffolds had the highest fluorescence intensity, whereas aligned BTO/PLLA composite fibrous scaffolds had a lower fluorescence intensity than the aligned neat PLLA samples (Figure 9B). The ALP activity assay result also showed similar trends (Figure 9C). The improved osteogenic response could be explained by the osteoinductive effect of inherent electrical properties derived from BTO NPs on stem cells as reported by other researchers.[50,51] However, the depressed osteogenic response in aligned composite fibrous scaffolds may be due to the slender cell shape, which is not conducive to osteogenic differentiation of BM-MSCs, despite the electrical effects present. These findings also implied that cell shape plays an essential role in regulating the differentiation of stem cells into specific tissues.[52,53] The mechanism may be related to the cytoskeleton changes inspired by contact-induced effects and the activation of intracellular-related signal proteins stimulated by electrotaxis.

It has been reported that changes in cell morphology may directly influence Rho family GTPases, which are related

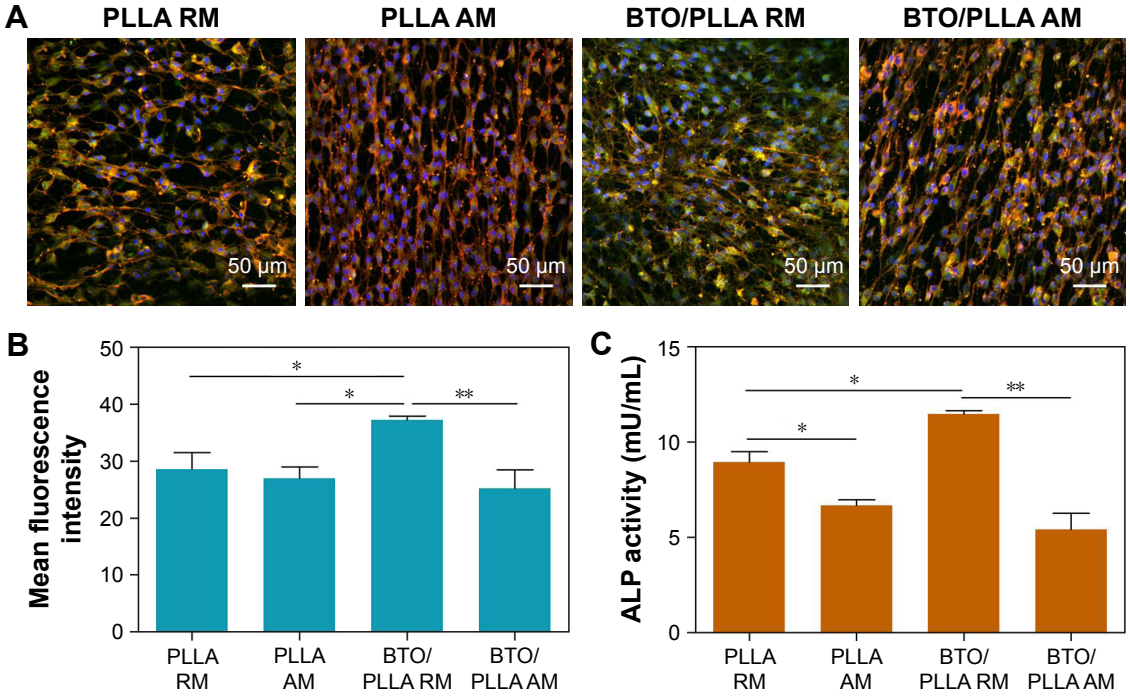

Figure 9 Osteogenic differentiation analysis of BM-MSCs on fibrous scaffolds.
Notes: (**A**) Representative immunofluorescence images of RUNX-2 (green), actin network (red), and nuclei (blue) in BM-MSCs cultured for 5 days. (**B**) Mean fluorescence intensity of positive RUNX-2 expression. (**C**) ALP activity of BM-MSCs cultured on different fibrous scaffolds for 5 days. (*$P<0.05$ and **$P<0.01$).
Abbreviations: ALP, alkaline phosphatase; BM-MSC, bone marrow mesenchymal stem cell; RUNX-2, runt-related transcription factor 2; PLLA RM, randomly oriented neat PLLA microfibers; PLLA AM, aligned neat PLLA microfibers; BTO/PLLA RM, randomly oriented BTO/PLLA microfibers; BTO/PLLA AM, aligned BTO/PLLA composite microfibers; PLLA, poly-(L-lactic acid); BTO, $BaTiO_3$.

in cell proliferation and differentiation.[54] A large amount of evidence has demonstrated that the RhoA/ROCK signaling pathway participates in osteogenic differentiation of MSCs via cytoskeletal reorganization.[55–57] In our previous study, it was also confirmed that the difference in the orientation of PLLA fibers leads to differences in the expression of ROCK2, a key indicator of the RhoA/ROCK signaling pathway.[9] Thus, It is speculated that the RhoA/ROCK pathway may be involved in the osteogenic differentiation effect of BTO/PLLA composite fibers on BM-MSCs. This could be a possible future research avenue that would focus on investigating the correlation between surface topography, dielectricity, and the signaling pathways involved in cellular responses. Our results demonstrated preliminarily that the topographical structure and electrical activity of randomly oriented electrospun BTO/PLLA composite fibrous scaffolds have combining effects on BM-MSC attachment, growth, and osteogenic response as described in Figure 10, suggesting a great potential for application in bone tissue engineering.

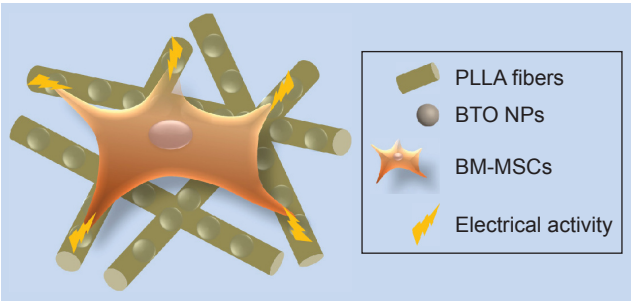

Figure 10 Illustration of the combining effects of topographical structure and electrical activity of randomly oriented electrospun BTO/PLLA composite fibrous scaffolds on BM-MSCs behavior.
Abbreviations: PLLA, poly-(L-lactic acid); BTO, $BaTiO_3$; BM-MSC, bone marrow mesenchymal stem cell; NP, nanoparticle.

Conclusion

In this work, randomly oriented and aligned electroactive BTO/PLLA composite fibrous scaffolds were fabricated by electrospinning. The incorporation of BTO NPs improved the surface roughness, surface hydrophilicity, and dielectric properties of fibrous scaffolds by electrical polarization during the electrospinning process. The randomly oriented composite fibrous scaffolds significantly encouraged polygonal spreading and early osteogenic differentiation of BM-MSCs, whereas aligned composite fibrous scaffolds increased cell elongation and discouraged osteogenic differentiation. Randomly fiber orientation and biomimetic electric activity had combining effects on osteogenic differentiation of BM-MSCs. Taken together, randomly oriented

BTO/PLLA composite fibrous scaffolds would have promising potential for application in bone regeneration.

Acknowledgments

This work was financially supported by the National Natural Science Foundation of China (Nos 51502006 and 81425007), the National High-tech R&D Program of China (No 2015AA033601), the Beijing Municipal Science & Technology Commission (No Z161100000116033), the National Science and Technology Program for Public Wellbeing (No S2013GMD200009), and the Educational Reform Project of Hunan Province (No JG2014A005). We thank Dr Fengyi Zhang and Dr Weiwei Liang from the Department of Geriatric Dentistry, Peking University School and Hospital of Stomatology, Beijing, People's Republic of China, for assistance with CLSM measurements.

Disclosure

The authors report no conflicts of interest in this work.

References

1. Lutolf MP, Gilbert PM, Blau HM. Designing materials to direct stem-cell fate. *Nature*. 2009;462(7272):433–441.
2. Discher DE, Mooney DJ, Zandstra PW. Growth factors, matrices, and forces combine and control stem cells. *Science*. 2009;324(5935):1673–1677.
3. Crowder SW, Leonardo V, Whittaker T, Papathanasiou P, Stevens MM. Material cues as potent regulators of epigenetics and stem cell function. *Cell Stem Cell*. 2016;18(1):39–52.
4. Guilak F, Cohen DM, Estes BT, Gimble JM, Liedtke W, Chen CS. Control of stem cell fate by physical interactions with the extracellular matrix. *Cell Stem Cell*. 2009;5(1):17–26.
5. Yin Z, Chen X, Chen JL, et al. The regulation of tendon stem cell differentiation by the alignment of nanofibers. *Biomaterials*. 2010;31(8):2163–2175.
6. Dang JM, Leong KW. Myogenic induction of aligned mesenchymal stem cell sheets by culture on thermally responsive electrospun nanofibers. *Adv Mater*. 2007;19:2775–2779.
7. He L, Liao S, Quan D, et al. Synergistic effects of electrospun PLLA fiber dimension and pattern on neonatal mouse cerebellum C17.2 stem cells. *Acta Biomater*. 2010;6(8):2960–2969.
8. Wang B, Cai Q, Zhang S, Yang X, Deng X. The effect of poly (L-lactic acid) nanofiber orientation on osteogenic responses of human osteoblast-like MG63 cells. *J Mech Behav Biomed Mater*. 2011;4(4):600–609.
9. Liu W, Wei Y, Zhang X, Xu M, Yang X, Deng X. Lower extent but similar rhythm of osteogenic behavior in hBMSCs cultured on nanofibrous scaffolds versus induced with osteogenic supplement. *ACS Nano*. 2013;7(8):6928–6938.
10. Yin Z, Chen X, Song HX, et al. Electrospun scaffolds for multiple tissues regeneration in vivo through topography dependent induction of lineage specific differentiation. *Biomaterials*. 2015;44:173–185.
11. Bassett CA, Becker RO. Generation of electric potentials by bone in response to mechanical stress. *Science*. 1962;137(3535):1063–1064.
12. Shamos MH, Lavine LS, Shamos MI. Piezoelectric effect in bone. *Nature*. 1963;197:81.
13. Marino A, Becker RO. Piezoelectric effect and growth control in bone. *Nature*. 1970;228:473–474.
14. LANG SB. Pyroelectric effect in bone and tendon. *Nature*. 1966;212:704–705.
15. Marchesano V, Gennari O, Mecozzi L, Grilli S, Ferraro P. Effects of lithium niobate polarization on cell adhesion and morphology. *ACS Appl Mater Interfaces*. 2015;7(32):18113–18119.
16. Li J, Mou X, Qiu J, et al. Surface charge regulation of osteogenic differentiation of mesenchymal stem cell on polarized ferroelectric crystal substrate. *Adv Healthc Mater*. 2015;4(7):998–1003.
17. Carville NC, Collins L, Manzo M, et al. Biocompatibility of ferroelectric lithium niobate and the influence of polarization charge on osteoblast proliferation and function. *J Biomed Mater Res A*. 2015;103(8):2540–2548.
18. Furuya KM, Morita Y, Tanaka K, Katayama T, Nakamachi E. Acceleration of osteogenesis by using barium titanate piezoelectric ceramic as an implant material. Proc. SPIE 7975, Bioinspiration, Biomimetics, and Bioreplication, 79750U (March 23, 2011). Available from: http://spie.org/Publications/Proceedings/Paper/10.1117/12.881858. Accessed May 18, 2015.
19. Ball JP, Mound BA, Nino JC, Allen JB. Biocompatible evaluation of barium titanate foamed ceramic structures for orthopedic applications. *J Biomed Mater Res A*. 2014;102(7):2089–2095.
20. Lopes HB, Santos Tde S, de Oliveira FS, et al. Poly(vinylidene-trifluoroethylene)/barium titanate composite for in vivo support of bone formation. *J Biomater Appl*. 2014;29:104–112.
21. Zhang X, Zhang C, Lin Y, et al. Nanocomposite membranes enhance bone regeneration through restoring physiological electric microenvironment. *ACS Nano*. 2016;10(8):7279–7286.
22. Meng S, Zhang X, Xu M, et al. Effects of deer age on the physicochemical properties of deproteinized antler cancellous bone: an approach to optimize osteoconductivity of bone graft. *Biomed Mater*. 2015;10(3):035006.
23. Tijing LD, Woo YC, Shim WG, et al. Superhydrophobic nanofiber membrane containing carbon nanotubes for high-performance direct contact membrane distillation. *J Membrane Sci*. 2016;502:158–170.
24. McHale GSNJ, Newton MI. Super-hydrophobic and super-wetting surfaces: analytical potential? *Analyst*. 2004;129:284–287.
25. Faia-Torres AB, Guimond-Lischer S, Rottmar M, et al. Differential regulation of osteogenic differentiation of stem cells on surface roughness gradients. *Biomaterials*. 2014;35(33):9023–9032.
26. Hu X, Park SH, Gil ES, Xia XX, Weiss AS, Kaplan DL. The influence of elasticity and surface roughness on myogenic and osteogenic-differentiation of cells on silk-elastin biomaterials. *Biomaterials*. 2011;32(34):8979–8989.
27. Thomas M, Arora A, Katti DS. Surface hydrophilicity of PLGA fibers governs in vitro mineralization and osteogenic differentiation. *Mater Sci Eng C Mater Biol Appl*. 2014;45:320–332.
28. Weaver JC, Astumian RD. The response of living cells to very weak electric fields: the thermal noise limit. *Science*. 1990;247(4941):459–462.
29. Burr HS, Northrop FS. Evidence for the existence of an electro-dynamic field in living organisms. *Proc Natl Acad Sci U S A*. 1939;25:284–288.
30. Shi G, Zhang Z, Rouabhia M. The regulation of cell functions electrically using biodegradable polypyrrole–polylactide conductors. *Biomaterials*. 2008;29:3792–3798.
31. Supronowicz PR, Ajayan PM, Ullmann KR, Arulanandam BP, Metzger DW, Bizios R. Novel current-conducting composite substrates for exposing osteoblasts to alternating current stimulation. *J Biomed Mater Res*. 2002;59(3):499–506.
32. Shao S, Zhou S, Li L, et al. Osteoblast function on electrically conductive electrospun PLA/MWCNTs nanofibers. *Biomaterials*. 2011;32(11):2821–2833.
33. Morvan J, Buyuktanir E, West JL, Jákli A. Highly piezoelectric biocompatible and soft composite fibers. *Appl Phys Lett*. 2012;100:1–9.
34. Luo H, Zhang D, Jiang C, Yuan X, Chen C, Zhou K. Improved dielectric properties and energy storage density of poly(vinylidene fluoride-co-hexafluoropropylene) nanocomposite with hydantoin epoxy resin coated $BaTiO_3$. *ACS Appl Mater Interfaces*. 2015;7(15):8061–8069.
35. Zhang X, Shen Y, Zhang Q, et al. Ultrahigh energy density of polymer nanocomposites containing $BaTiO_3$@TiO_2 nanofibers by atomic-scale interface engineering. *Adv Mater*. 2015;27(5):819–824.

36. Zhang X, Shen Y, Xu B, et al. Giant energy density and improved discharge efficiency of solution-processed polymer nanocomposites for dielectric energy storage. *Adv Mater*. 2016;28(10):2055–2061.
37. Hu PH, Shen Y, Guan YH, et al. Topological-structure modulated polymer nanocomposites exhibiting highly enhanced dielectric strength and energy density. *Adv Funct Mater*. 2014;24:3172–3178.
38. Liu B, Chen L, Shao C, et al. Improved osteoblasts growth on osteomimetic hydroxyapatite/$BaTiO_3$ composites with aligned lamellar porous structure. *Mater Sci Eng C Mater Biol Appl*. 2016;61:8–14.
39. Park YJ, Hwang KS, Song JE, Ong JL, Rawls HR. Growth of calcium phosphate on poling treated ferroelectric $BaTiO_3$ ceramics. *Biomaterials*. 2002;23(18):3859–3864.
40. Rahmati S, Basiriani MB, Rafienia M, Yaghini J, Raeisi K. Synthesis and in vitro evaluation of electrodeposited barium titanate coating on Ti6Al4V. *J Med Signals Sens*. 2016;6(2):106–111.
41. Shamos MH, Lavine LS. Physical bases for bioelectric effects in mineralized tissues. *Clin Orthop Relat Res*. 1964;35:177–188.
42. Dubey AKB, Basu B, Balani K, Guo R, Bhalla AS. Multifunctionality of perovskites $BaTiO_3$ and $CaTiO_3$ in a composite with hydroxyapatite as orthopedic implant materials. *Integr Ferroelectr*. 2011;131:119–126.
43. Knauth P. Inorganic solid Li ion conductors: an overview. *Solid State Ionics*. 2009;180:911–916.
44. Zhang X, Chen W, Wang J, et al. Hierarchical interfaces induce high dielectric permittivity in nanocomposites containing TiO_2@$BaTiO_3$ nanofibers. *Nanoscale*. 2014;6(12):6701–6709.
45. Tsimbouri PM, McMurray RJ, Burgess KV, et al. Using nanotopography and metabolomics to identify biochemical effectors of multipotency. *ACS Nano*. 2012;6(11):10239–10249.
46. Yang J, McNamara LE, Gadegaard N, et al. Nanotopographical induction of osteogenesis through adhesion, bone morphogenic protein cosignaling, and regulation of microRNAs. *ACS Nano*. 2014;8(10):9941–9953.
47. Farooque TM, Camp CH, Tison CK, Kumar G, Parekh SH, Simon CG. Measuring stem cell dimensionality in tissue scaffolds. *Biomaterials*. 2014;35(9):2558–2567.
48. Peng R, Yao X, Ding JD. Effect of cell anisotropy on differentiation of stem cells on micropatterned surfaces through the controlled single cell adhesion. *Biomaterials*. 2011;32(32):8048–8057.
49. Zhao L, Liu L, Wu Z, Zhang Y, Chu PK. Effects of micropitted/nanotubular titania topographies on bone mesenchymal stem cell osteogenic differentiation. *Biomaterials*. 2012;33(9):2629–2641.
50. Bagchi A, Meka SR, Rao BN, Chatterjee K. Perovskite ceramic nanoparticles in polymer composites for augmenting bone tissue regeneration. *Nanotechnology*. 2014;25(48):485101.
51. Rocca A, Marino A, Rocca V, et al. Barium titanate nanoparticles and hypergravity stimulation improve differentiation of mesenchymal stem cells into osteoblasts. *Int J Nanomedicine*. 2015;10:433–445.
52. Kumar G, Tison CK, Chatterjee K, et al. The determination of stem cell fate by 3D scaffold structures through the control of cell shape. *Biomaterials*. 2011;32(35):9188–9196.
53. Andersson AS, Backhed F, von Euler A, Richter-Dahlfors A, Sutherland D, Kasemo B. Nanoscale features influence epithelial cell morphology and cytokine production. *Biomaterials*. 2003;24(20):3427–3436.
54. McBeath R, Pirone DM, Nelson CM, Bhadriraju K, Chen CS. Cell shape, cytoskeletal tension, and RhoA regulate stem cell lineage commitment. *Dev Cell*. 2004;6(4):483–495.
55. Hu J, Liu X, Ma PX. Induction of osteoblast differentiation phenotype on poly(L-lactic acid) nanofibrous matrix. *Biomaterials*. 2008;29(28):3815–3821.
56. Yang-Kao Wang XY, Cohen DM, Wozniak MA, et al. Bone morphogenetic protein-2-induced signaling and osteogenesis is regulated by cell shape, RhoA/ROCK, and cytoskeletal tension. *Stem Cells Dev*. 2011;21(7):1176–1186.
57. Andalib MN, Lee JS, Ha L, Dzenis Y, Lim JY. The role of RhoA kinase (ROCK) in cell alignment on nanofibers. *Acta Biomater*. 2013;9(8):7737–7745.